Journal of
Plankton Research

academic.oup.com/plankt

J. Plankton Res. (2021) 43(2): 126–141. First published online March 17, 2021 doi:10.1093/plankt/fbab009

ORIGINAL ARTICLE

Two versions of short-term phytoplankton ecophysiology and taxonomic assemblages in the Arctic Ocean's North Water (Canada, Greenland)

NATHALIE JOLI[1,2,†], THOMAS LACOUR[1,‡], NASTASIA J. FREYRIA[1,2], SARAH-JEANNE ROYER[3,§], MARCEL BABIN[1] AND CONNIE LOVEJOY[1,2,*]

[1]DÉPARTEMENT DE BIOLOGIE, QUÉBEC OCÉAN AND TAKUVIK JOINT INTERNATIONAL LABORATORY (UMI 3376), UNIVERSITÉ LAVAL (CANADA) - CNRS (FRANCE), UNIVERSITÉ LAVAL, QUÉBEC, QC G1V 0A6, CANADA, [2]INSTITUT DE BIOLOGIE INTÉGRATIVE ET DES SYSTÈMES (IBIS), UNIVERSITÉ LAVAL, QUÉBEC, QC G1V 0A6, CANADA AND [3]INSTITUTE DE CIÈNCIES DEL MAR, CSIC, PASSEIG MARÍTIM DE LA BARCELONETA 37-49, 08003 BARCELONA, SPAIN

*CORRESPONDING AUTHOR: connie.lovejoy@bio.ulaval.ca

[†]PRESENT ADDRESS: INSTITUT DE BIOLOGIE DE L'ÉCOLE NORMALE SUPÉRIEURE (IBENS), CNRS UMR 8197, 46 RUE D'ULM, 75 005 PARIS, FRANCE

[‡]PRESENT ADDRESS: LABORATOIRE PHYSIOLOGIE ET BIOTECHNOLOGIE DES ALGUES (PDG-RBE-BRM-LPBA), CENTRE ATLANTIQUE, RUE DE L'ILE D'YEU, BP 21105, 44 311 NANTES, CEDEX 03, FRANCE

[§]PRESENT ADDRESS: MARINE BIOLOGY RESEARCH DIVISION, SCRIPPS INSTITUTION OF OCEANOGRAPHY, UNIVERSITY OF CALIFORNIA, SAN DIEGO, 9500 GILMAN DRIVE, LA JOLLA, CA 92093-0202, USA

Received November 18, 2019; editorial decision January 15, 2021; accepted January 15, 2021

Corresponding editor: Lisa Campbell

Photosynthetic performance in open marine waters is determined by how well phytoplankton species are adapted to their immediate environment and available light. Although there is light for 24 h a day during the Arctic summer, little is known about short-term (h) temporal variability of phytoplankton photosynthetic performance in Arctic waters. To address this, we sampled the North Water (76.5°N) every 4 h over 24 h at two stations on the East and West sides that are influenced by different water masses and current conditions. We specifically investigated phytoplankton pigments, the xanthophyll cycle (XC), which is an indication of photoprotective capacity, and photosynthesis–irradiance (PE) response curves, at the surface and 20 m depth. The photophysiological parameters on the two sides differed along

available online at academic.oup.com/plankt

© The Author(s) 2021. Published by Oxford University Press. All rights reserved. For permissions, please e-mail: journals.permission@oup.com.

Downloaded from https://academic.oup.com/plankt/article/43/2/126/6174319 by guest on 19 April 2024

with the taxonomic signal derived from accessory pigments. On both sides, surface XC pigments showed high photoprotection capacity with the dinodinoxanthin–diatoxanthin (DD) and the violaxanthin, antheraxanthin and zeaxanthin cycles correlated with incoming radiation. The PE results showed that communities dominated by small flagellates on the western side performed better compared to diatom dominated communities on the eastern side. We conclude that phytoplankton and photosynthetic capacity differed consistent with known hydrography, with implications for a changing Arctic.

KEYWORDS: xanthophylcycle; photoprotection; phytoplankton pigments; PE curves; Pikialasorsuaq

INTRODUCTION

The light-harvesting capacity of marine pelagic photosynthetic communities has long been associated with temporal changes in the physical oceanographic environment (van de Poll *et al*., 2016), and phytoplankton species assemblages are thought to be selected for and adapted to local conditions (Edwards *et al*., 2015). However, to date, most studies on phytoplankton photophysiology have focused on a few species grown under laboratory conditions. Over the last few decades, photosynthesis versus irradiance (PE) curves have proved to be invaluable for estimating *in situ* primary production (Bouman *et al*., 2018, 2020) and the need for more *in situ* data from the Arctic is particularly critical because ongoing climate change is already impacting the surface mixed layer and average available light (Arrigo *et al*., 2010). These factors play a role in selecting dominant phytoplankton species, and ongoing climate change has already altered the balance of diatoms and small green algae in parts of the Arctic Ocean (Li *et al*., 2009; Blais *et al*., 2017). Continuing change will affect the biogeography and biodiversity of Arctic food webs, which are dependent on phytoplankton productivity (Polyakov *et al*., 2018).

Across the Arctic, nutrient and light regimes select species from a pool of pan-Arctic specialists adapted to cold temperatures and arguably to low average light levels since light is limiting for much of the year (Monier *et al*., 2015; Kalenitchenko *et al*., 2019). During summer, when light is available in the surface waters, nutrients are depleted, and biomass accumulates below the mixed layer (Martin *et al*., 2010), with most of the phytoplankton living under low light conditions (Monier *et al*., 2015). Given the habitual low light environment, key questions center on maintaining photosynthesis under low and high light conditions and whether Arctic phytoplankton species assemblages maintain their capacity for photoprotection.

Phytoplanktons have a suite of responses to adjust to short-term changes in light availability, which includes photoacclimation processes. This involves many cellular components, occurring over a broad range of time scales (from seconds to days), allowing the optimization of activities such as photosynthesis, respiration, growth and division, when faced with changing irradiance (Herzig and Dubinsky, 1993; Anning *et al*., 2000; Raven and Geider, 2003). Although short-term changes in photophysiology have been occasionally examined *in situ* (Harding *et al*., 1981; Doblin *et al*., 2011), there are few published studies at the scale of hours documenting changes in natural populations in the open ocean. Most such studies to date have focused on tropical and temperate regions dominated by cyanobacteria (Huang *et al*., 1990; Cai *et al*., 2015), where phytoplankton growth cycles are highly synchronized with light cycles. For example, offshore of Monterey Bay gene expression by *Synechococcus* and the picoeukaryote *Ostreococcus* showed marked diel patterns (Ottesen *et al*., 2013), consistent with laboratory-based studies of cultures under alternating dark–light cycles (Bruyant *et al*., 2005; Apple *et al*., 2011; Dron *et al*., 2012; Dupont *et al*., 2015). There is evidence from laboratory experiments that polar diatoms retain their capacity to adjust to daily rhythms in photon flux. For example, *Thalassiosira gravida* has a remarkable photoacclimatory plasticity, which is supported by sustained non-photochemical quenching (NPQ) at moderately low light (Lacour *et al*., 2017, 2018). An investment in photoprotective mechanisms via the xanthophyll cycle (XC) seems to be successful, in view of the seasonal predominance of such diatoms in polar waters. However, knowledge of short-term *in situ* changes in photoprotective response at latitudes above the Arctic Circle in mixed phytoplankton communities is sparse. Alou-Font *et al*. (2016) showed that some pigments vary with the light cycle in natural communities from the western Canadian Arctic, and other studies suggest similar responses in sub-Antarctic and Antarctic waters (Doblin *et al*., 2011; Russo *et al*., 2018). However, diel pigment periodicity does not necessarily propagate to photophysiological parameters such as the light saturation coefficient (E_K) or the rate of carbon fixation estimated from PE curves, and there is a need to examine phytoplankton response from oceanographically varied systems in the Arctic.

Pikialasorsuaq (the Inuit name for Northern Baffin Bay) includes the North Water Polynya region between Greenland and Ellesmere Island (Canada) and is one of the most productive marine systems in the Arctic, supporting large marine bird and mammal populations (Karnovsky and Hunt, 2002; Heide-Jorgensen *et al*., 2013). This

Downloaded from https://academic.oup.com/plankt/article/43/2/126/6174319 by guest on 19 April 2024

productivity is associated with a longer open water season and complex hydrography that fuels a short diatom-based food chain (Booth *et al*., 2002). However, the microbial eukaryotic communities on the two sides of the North Water region are often taxonomically different, with microbial communities selected by local oceanographic conditions (Joli *et al*., 2018). Physical oceanographic processes on the two sides differ, with strong southward currents and an input of Central Arctic waters on the West side (Canada), and the influence of northward flowing deeper Atlantic overlain by fresher Arctic ice melt-influenced water near Greenland on the East side (Bâcle *et al*., 2002), suggesting separate Arctic seascapes (Kavanough *et al*., 2016) on the two sides. Although nearly annual sampling has been carried out along a 76.5°N transect (referred to as line 100) of the North Water region since 2005 (Ardyna *et al*., 2011; Marchese *et al*., 2017), the short-term (h) changes in communities, pigment ratios and photophysiological parameters have not been investigated. To address this, we repeatedly sampled on the East and West sides of the North Water over a full day (24 h) on two separate days. Specifically, we carried out bulk community measurements of photosynthetic capacity, by way of PE curves to test for short-term (every 4 h) changes in phytoplankton photophysiology (Sakshaug *et al*., 1997; Huot *et al*., 2007; Huot *et al*., 2013). We identified phytoplankton pigments using high-pressure liquid chromatography (HPLC) as a means to categorize photosynthetic communities in the different samples (Roy *et al*. 2011). We then examined XC pigments to evaluate how *in situ* communities responded to increased light levels over the day (Brunet *et al*., 2011). To further identify the phytoplankton community, we mined the V4 18S ribosomal RNA (rRNA) amplicon data reported previously (Joli *et al*., 2018) from samples collected in conjunction with the present study. Multivariate analysis was then used to construct a more global view of the short-term phytoplankton ecophysiology linked to the prevailing phytoplankton communities and to light regimes within the two distinct arctic seascapes (Salazar *et al*., 2019). The differences between sides and depths highlighted potential impact of surface freshening and sea ice loss, which influence the mixed layer depth (MLD) and light fields in polar environments. Our results suggest that diatoms were less able to adjust to high light compared to small flagellates.

METHOD

Field sampling and analysis

Sampling was carried onboard the CCGS Amundsen in August 2013 as previously described in Joli *et al*. (2018). The temporal stations were initiated on the western (ArcticNet Station 101) and eastern (ArcticNet Station 115) sides of the polynya region, which will be referred to as WEST Stations T_1 to T_7 and EAST Stations T_1 to T_7, respectively (Fig. 1). Temporal stations were sampled every ca. 4 h over nearly 24 h (Table I, Supplementary Table S1). The locations varied due to the ship following a drogue that had been suspended to 20 m. Physical oceanographic data were collected on the downward casts using a Rosette system equipped with a conductivity, temperature, depth (CTD; SBE-911 CTD, Sea-Bird Electronics Inc.) profiler and sensors for chlorophyll fluorescence (Seapoint Sensors Inc.) oxygen (Seabird SBE-43), fluorescent-colored dissolved organic matter (*f*CDOM; Wetlabs ECO) and photosynthetically available radiation (PAR; Biospherical Instruments QCP3200) sensors. The oxygen sensor was calibrated onboard against Winkler titrations. Specifically, for our analysis, PAR for the 20 m samples was taken directly from the CTD data. Average PAR (E_{ave}) for the surface samples (Table I) was calculated by first determining the depth of the upper mixed layer ($\mathcal{Z}$) from the Brunt–Väisälä frequency and then estimating the extinction coefficient (K) from PAR from 0 m to $\mathcal{Z}$:

$$E_{ave} = 100 / (K \times \mathcal{Z}).$$

Regional above water PAR data over the two 24-h periods was collected atop the wheelhouse using a PAR light sensor (Pyranometer, Kipp & Zonen). Cloud cover at the time of sampling was estimated as oktas (eighths of the sky covered) as an additional indicator of light variability during the day.

Water samples from the surface and at 20 m, which corresponded to the bottom of the Polar Mixed Layer (PML), were collected on the upcasts, using 12-L Niskin-type bottles mounted on the Rosette. All surface samples were taken, with bottles closed about 1 m below the surface. Seas were calm the day of sampling for WEST side and waves (<1 m) the day of sampling of the EAST side (Supplementary Fig. S1).

Samples for nutrients were collected every 10 m as previously described (Blais *et al*., 2017; Joli *et al*., 2018). Nitrate + nitrite, silicate and phosphate were analyzed on board using a Bran-Luebbe 3 autoanalyzer using standard protocols (Grasshoff *et al*., 2009). For pigments, including Chl *a*, water was collected into 2-L brown polycarbonate (PC) bottles and filtered through GF/F filters in the dark under low vacuum pressure. The filters were flash frozen in liquid nitrogen and stored at −80°C until HPLC analysis. Sample water for photosynthetic parameters was collected and analyzed following Huot *et al*. (2013). Briefly, PE curves were carried out using a radial photosynthetron equipped with a metal halide

Downloaded from https://academic.oup.com/plankt/article/43/2/126/6174319 by guest on 19 April 2024

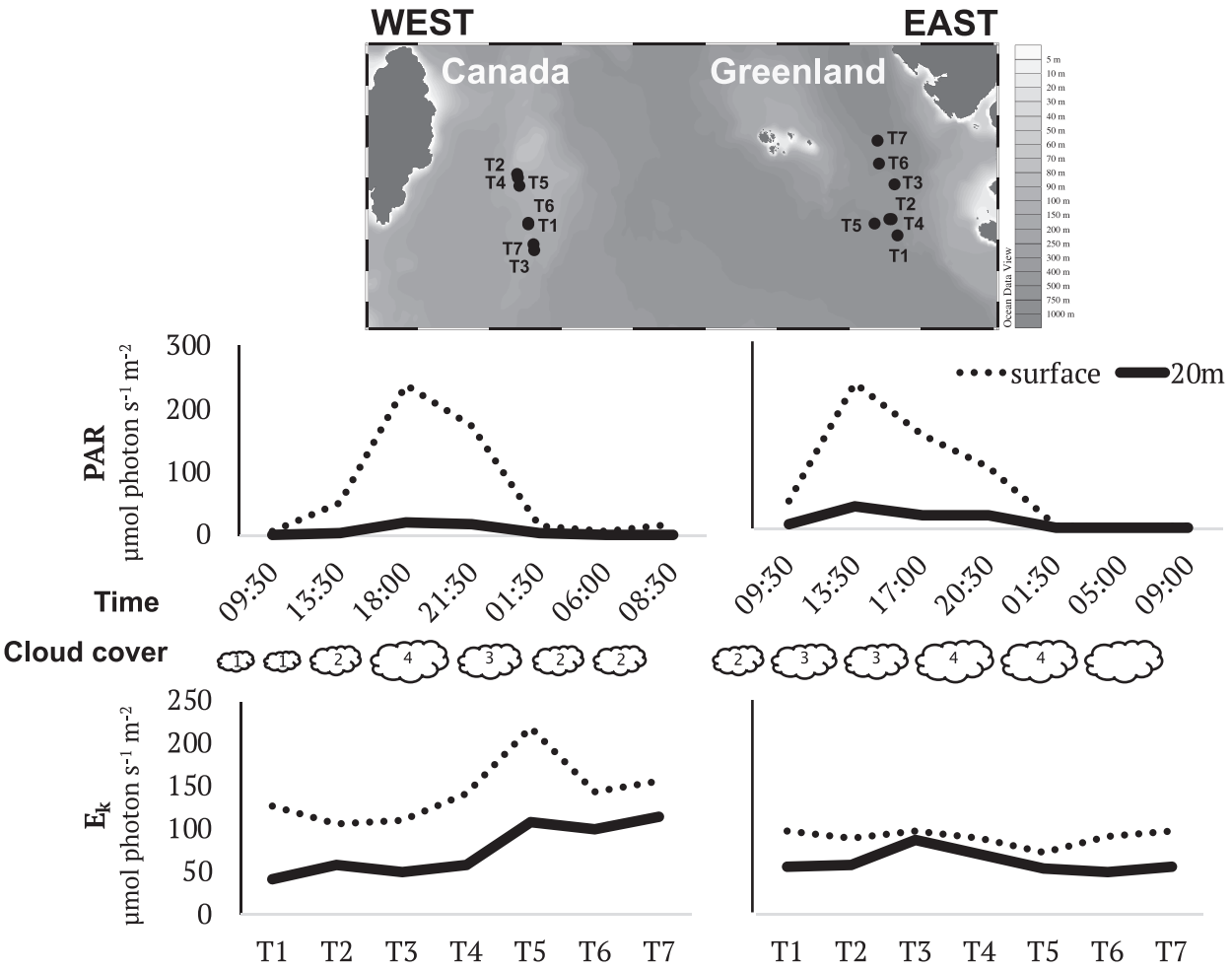

Fig. 1. Variability over 24 h, the two sides of the North Water region at the time of sampling. Upper panel (map) indicates CTD cast and water collection sites on the western (WEST stations) side and the eastern side (EAST stations). Samples were collected every 4 h beginning at 9:30 UTC (WEST) and at 9:00 UTC (EAST). Stations from the two sides are listed by time of sampling starting with T_1, T_2, T_3, T_4, T_5, T_6, T_7. The center panels show PAR over the day at each station and depth (surface and 20 m). Bottom panels show the photophysiological parameter E_k from the stations for the two depth categories on the respective sides. Cloud cover estimates during sample collection from direct observations are indicated as eighths of sky coverage. Map created with Ocean Data View (version 4.7.8).

lamp, and light levels followed the exponential model described in Huot *et al*. (2007). For the PE curves, irradiance was measured in the photosynthetron using a scalar sensor (Biospherical Instruments Inc., USA). The initial slope alpha (α^B) and maximum photosynthesis (P^B_{max}) were normalized to the total (non-pheophytin corrected) Chl *a* concentrations determined by HPLC (see below). We fit the data following the Platt model (Bouman *et al*., 2018) to obtain the light-saturated rate of photosynthesis, the initial slope of the PE curve and the photoinhibition parameter, normalized to Chl *a* (P^B_{max}, α^B and β^B, respectively) and the light-saturation parameter (E_K) of the carbon fixation rate versus incubation irradiance curve.

Samples for phytoplankton enumeration were collected for Flow cytometry (FCM) directly from the Niskin-type bottles and fixed by adding 90 µL of 25% glutaraldehyde to 1.8 mL of seawater for a final concentration of 1% (v/v). Preserved samples were left for 30 min at 4°C in the dark, flash frozen in liquid nitrogen and stored at−80°C. Nucleic acid (RNA) samples were collected from 20 m from the same casts, this water was sequentially filtered through 3-µm pore size PC filters (large fraction) and 0.2-µm Sterivex® filters (small fraction) as described previously (Joli *et al*., 2018).

Laboratory procedures

Pico- and nano-phytoplankton concentrations were obtained from FCM counts performed following Belzile *et al*. (2008) with modifications. Specifically, cell concentrations, fluorescence and scatter properties were measured using a BD Accuri C6 flow cytometer equipped with

Downloaded from https://academic.oup.com/plankt/article/43/2/126/6174319 by guest on 19 April 2024

Table I: Characteristics of the two stations at two depths. Time Station categories (T) as in the main text; Brunt-Väisälä frequency (N^2, in 10^{-3} s^{-2}); upper mixed layer depth (MLD, in m); photosynthetically active radiation (PAR) as either surface mixed layer averages (Surface) or in situ (20 m), in μmol photons m^{-2} s^{-1}; chlorophyll a (Chl a) from HPLC in μg L^{-1}; Chl b as a molar proportion of Chl a; light-saturation parameter (E_K, in μmol photons m^{-2} s^{-1}); light use efficiency parameter (α^B, in g C (g Chl a)$^{-1}$ h^{-1} (μmol photons m^{-2} s^{-1})$^{-1}$); maximum photosynthetic rate (P^B_{max}, in g C (g Chl a)$^{-1}$ h^{-1}); and the beta parameter (β^B, in g C (g Chl a)$^{-1}$ h^{-1} (μmol photons m^{-2} s^{-1})$^{-1}$). Data not applicable (na).

Stn_T	N^2	MLD m	Chl *a*	Chl *b*	PAR	E_K	α^B	P^B_{max}	β^B
Surface									
WEST_T_1	2.16	11	0.314	0.361	11.4	126.45	0.010	1.25	0.011
WEST_T_2	0.155	17	0.238	0.316	47.3	106.64	0.013	1.39	0.002
WEST_T_3	1.33	16	0.504	0.309	225.5	110.52	0.012	1.33	0.018
WEST_T_4	0.767	13	0.368	0.276	214.8	142.03	0.009	1.28	0.052
WEST_T_5	0.818	18	0.418	0.311	22.4	218.70	0.008	1.83	0.047
WEST_T_6	1.79	15	0.419	0.310	8.5	143.43	0.011	1.54	0.017
WEST_T_7	1.25	17	0.456	0.309	18.6	156.10	0.008	1.24	0.015
EAST_T_1	2.92	14	0.212	0.154	44.9	94.21	0.010	0.98	0.001
EAST_T_2	5.46	9	0.159	0.152	225.5	85.72	0.012	1.07	0.002
EAST_T_3	2.62	12	0.202	0.135	183.3	93.11	0.012	1.08	0.002
EAST_T_4	2.81	16	0.185	0.135	191.2	85.46	0.012	1.04	0.002
EAST_T_5	2.82	17	0.211	0.142	9.4	69.95	0.010	0.68	0.000
EAST_T_6	2.69	19	0.211	0.151	2.3	86.96	0.011	0.97	0.001
EAST_T_7	2.79	19	0.186	0.159	8.6	94.21	0.013	1.22	0.003
20 m									
WEST_T_1	na	na	0.408	0.075	0.8	40.43	0.017	0.68	0.018
WEST_T_2	na	na	0.329	0.327	4.4	58.17	0.016	0.95	0.011
WEST_T_3	na	na	0.323	0.270	20.9	49.31	0.017	0.81	0.006
WEST_T_4	na	na	0.380	0.267	17.0	57.57	0.014	0.79	0.056
WEST_T_5	na	na	0.329	0.314	2.1	107.94	0.016	1.70	0.029
WEST_T_6	na	na	0.355	0.310	0.6	99.80	0.013	1.32	0.032
WEST_T_7	na	na	0.378	0.374	1.6	114.27	0.012	0.84	0.025
EAST_T_1	na	na	0.475	0.049	6.1	54.04	0.017	0.92	0.002
EAST_T_2	na	na	0.278	0.088	33.8	55.59	0.010	0.56	0.000
EAST_T_3	na	na	0.252	0.239	19.8	83.01	0.011	0.92	0.002
EAST_T_4	na	na	0.208	0.248	21.4	67.58	0.014	0.95	0.002
EAST_T_5	na	na	0.549	0.122	1.0	51.05	0.013	0.66	0.002
EAST_T_6	na	na	0.360	0.146	0.2	46.97	0.017	0.78	0.001
EAST_T_7	na	na	0.429	0.083	0.9	53.38	0.017	0.91	0.003

a 14.7 mW 640 nm Diode Red Laser and 20 mW 488 nm Solid State Blue Laser. To distinguish picoplankton and nanoplankton, the gate was adjusted using the scatter characteristics of 2-μm Fluoresbrite™ beads diluted in filtered seawater. The three replicates of this standard were run in separate wells in the 96-well plate automated system.

For the HPLC analysis, pigments were extracted in 95% methanol and separated with a Accela 600 HPLC system (Thermo Fisher Scientific) on a reverse-phase Hypersil Gold C-8 column and a solvent gradient containing methanol, aqueous pyridine, acetone and acetonitrile (Zapata *et al*., 2000). An Accela PDA detector recorded chromatograms at 450 nm and pigment spectra over 350–800 nm wavelengths. A Finnigan Surveyor FL Plus fluorescence detector with 440 nm excitation and 650 nm emission (optimized for Chl *a*) was used to identify and quantify Chl pigments. The system was calibrated by repeated injections of 30 pigment standards (Sigma-Aldrich or DHI LAB products). ChromeQuest software was used to identify and quantify the concentration of the pigments. The photodiode array spectrum of each peak was checked against the reference spectra of standards or against the reference spectra given in Roy *et al*. (2011) for pigments for which there are no standards. As an indicator of photophysiological protection in the communities, we calculated the de-epoxidation state (DES), from the diadinoxanthin–diatoxanthin (DD) cycle (DES = Dt/(Dt + Dd) used by diatoms and in Xanthophyceae, Haptophyceae and Dinophyceae and from the violaxanthin, antheraxanthin and zeaxanthin (VAZ) cycle (DES = (Z + A)/(Z + A + V)) found in higher plants, green (Chlorophyta) and brown algae (Phaeophyceae) and in the Chromeraceae specifically *Chromera velia* a member of an Alveolate clade (Goss and Lepetit, 2015).

Downloaded from https://academic.oup.com/plankt/article/43/2/126/6174319 by guest on 19 April 2024

Microbial eukaryotes were identified by targeting the V4 region of 18S rRNA gene to obtain 300 bp paired-end sequence reads. RNA was extracted from the stored filters, converted to cDNA and sequenced as previously described (Joli *et al*., 2018). Briefly, for this study, the reads were processed with UPARSE (Edgar, 2013), as implemented in Logares *et al*. (2017). All steps for assembly, quality check, operational taxonomic unit (OTU) clustering and taxonomic assignment are reported in Joli *et al*. (2018). To facilitate comparison with the pigment data, OTUs belonging to non-photosynthetic taxa were removed from the larger data set. We also removed dinoflagellate reads since in the Arctic many are heterotrophic or mixotrophic non-peridinin taxa. For the present study, the large and small fraction results were combined after checking that this mathematical operation did not mask or over represent a given OTU. Amplicon results are in the NCBI GenBank Sequence Read Archive under the BioProject PRJNA383398.

Statistical analyses

Dissimilarities among samples based on pigment profiles was determined by Bray–Curtis distance and Unweighted Pair Group Method with Arithmetic Mean carried out using the PAleontological STatistics (PAST version 3.11) software and verified using R (Rcore, v.3.4.2). One-way analysis of variance (ANOVA) (parametric) and Kruskal–Wallis (non-parametric) tests for equality of means between samples were also carried out in PAST. The rRNA reads, grouped into OTUs from the 20 m samples, were similarly clustered as described earlier (Joli *et al*., 2018). To compare pigments with the species, we applied cannonical correspondence analysis (CCA) using *cca()* functions in the *Vegan* package performed using R (v.3.4.2) and R studio (v.1.1.419). The pigment and species variables that best explained variability in the CCA were selected using *envfit()* functions in *Vegan*, and automatic forward selection with adjusted coefficient determination (R^2 adj.) were used to build optimal model. To identify the pigments associated with the samples, against depth, PAR and the photophysiology characteristics, we performed the same analysis but with all stations and depths and with the photophysiological and environmental variables selected by *envfit()* and forward selection.

RESULTS

Environmental conditions and photosynthetic biomass

Physical oceanographic and nutrient depth profiles of the two stations were reported previously (Joli *et al*. 2018). Briefly, for the specific samples here, for the Canadian side (WEST) samples, surface temperatures ranged from 3.6 to 4.3°C, with an average of 4.1°C, and 20 m temperatures ranged from 2.6 to 4.0°C, with an average of 3.5°C. For the Greenland side (EAST), surface samples were fairly uniform around 3.5°C and the 20 m temperatures range was 0.1–3.9°C, with an average of 2.2°C (Table I, Fig. 2). Nitrate concentrations were low in both surface and 20 m at both EAST and WEST stations, ranging from 0.09 to 0.28 μM, with phosphate concentrations relatively high with a range of 0.16–0.56 μM. Overall, the average biotic and abiotic parameters measured were relatively similar the respective 24 h at both stations. At 20 m, there was an exception for T_1 and T_2 on the eastern side, where the halocline and underlying Atlantic water was closer to the surface (Fig. 2). Although MLD from the Brunt–Väisälä frequency delineating the surface mixed layer was similar on both sides (Table I), vertical profiles of potential density highlighted a sharper halocline and more isolated mixed surface layer for EAST stations (Supplementary Fig. S1). Average surface Chl *a* concentrations from HPLC were significantly higher in the WEST stations (0.435 pmol L^{-1}) compared to the EAST stations (0.218 pmol L^{-1}) (ANOVA, $P < 0.001$), while concentrations from 20 m were similar, with averages of 0.400 and 0.408 pmol L^{-1}, for the WEST and EAST stations, respectively (Table I, Supplementary Table S2). Over the 24-h sampling, surface Chl *a* from the EAST stations varied from 0.238 to 0.504 μg L^{-1}. Values from 20 m varied less ranging from 0.323 and 0.408 μg L^{-1}. For the EAST stations, surface Chl *a* values ranged from 0.159 to 0.211 μg L^{-1}, while concentrations from 20 m samples were from 0.208 to 0.549 μg L^{-1} (Table I).

For both sides at 20 m, concentrations of eukaryotic phytoplankton cells from FCM ranged from 1.8 to 9.7×10^3 cells mL^{-1}, but with similar averages on the two sides at ca. 6.2×10^3 cells mL^{-1}, putative cyanobacteria were <0.1% of counts. The lowest cell counts were at T_1 for the WEST (Supplementary Fig. S2). This sample was also exceptional and was the only sample from the WEST stations where picophytoplankton did not account for over two-thirds of the cells. The mix of nano- and picoplankton for the EAST stations was more evenly split, with more than one-third of cells classified as nanoplankton. The cytograms from FCM forward scatter tended to be dispersed, and pico- and nanoplankton determination was based on standard bead scatter (Supplementary Fig. S2).

Photosynthetic capacity

PE curves generally fit the Platt model (Bouman et al., 2018) with little evidence of photoinhibition (Table I,

Downloaded from https://academic.oup.com/plankt/article/43/2/126/6174319 by guest on 19 April 2024

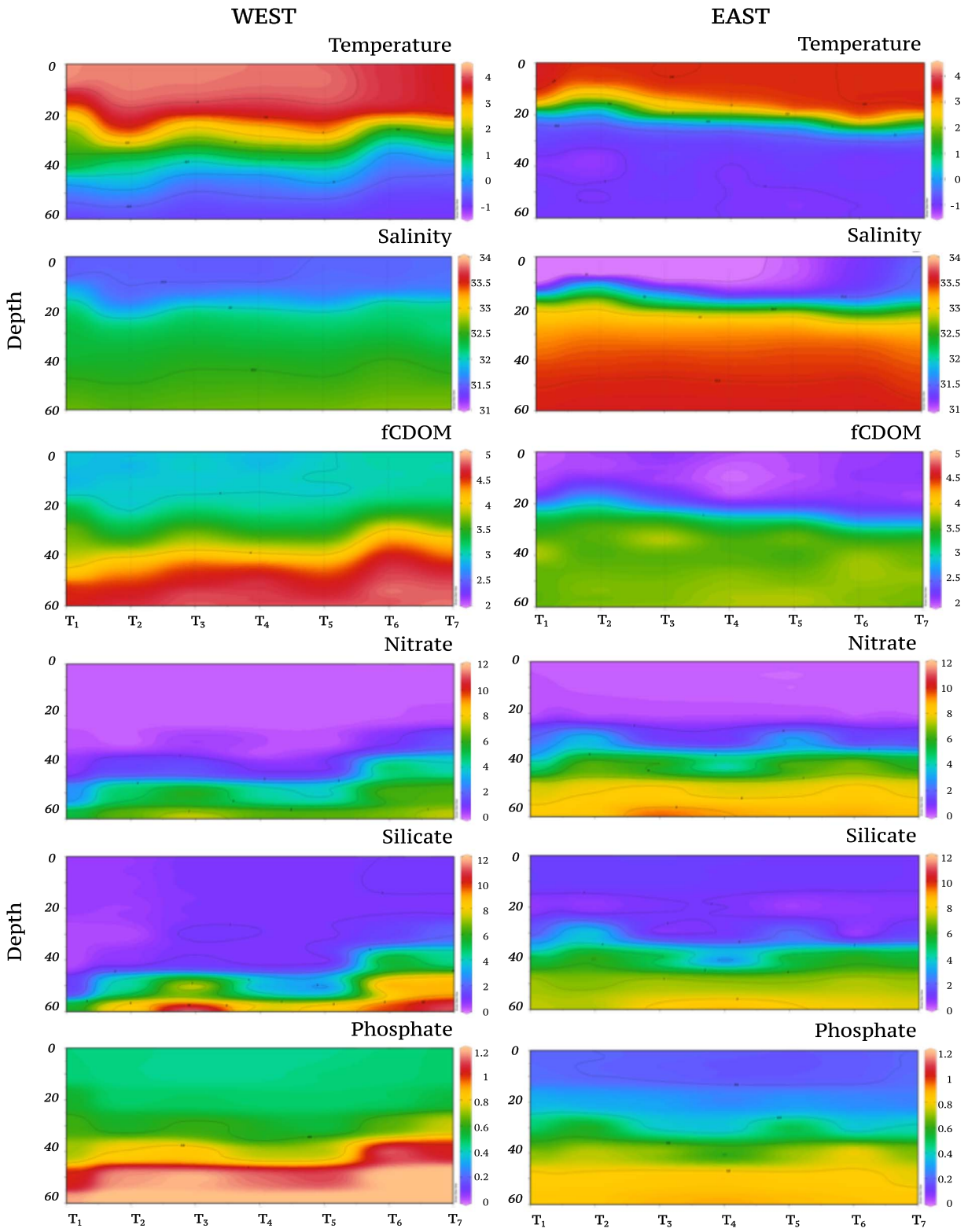

Fig. 2. Vertical sections of the upper 60 m for environmental parameters following the temporal sampling track from T_1 to T_7 for the two sides (WEST and EAST). Temperature, salinity and CDOM from CTD data at 1-m intervals. The nutrients, nitrate + nitrite (nitrate) and phosphate concentrations were from discrete samples take every 10 m. Sampling time points on the respective sides are indicated by the station designation (T_1 to T_7) for the respective sides (see Figure 1). Figures made using Ocean Data View (ODV version 4.7.8).

Downloaded from https://academic.oup.com/plankt/article/43/2/126/6174319 by guest on 19 April 2024

Supplementary Fig. S3a and b). The light-saturation parameter (E_K) from the PE experiments was generally greater for the higher average irradiance (E_{ave}) surface samples compared to 20 m on the same side. (Table I, Fig. 1, Supplementary Fig. S4). The difference between depths was less pronounced for the EAST stations, where the range of values was smaller (Supplementary Fig. S4). The WEST stations' E_K (in μmol photons m^{-2} s^{-1}) ranged from 106 to 218 at the surface and from 40 to 114 in the 20 m samples. For the EAST stations, E_K values varied less, with values from 70 to 106 at the surface and from 58 to 90 for 20 m samples. The ANOVA several samples test indicated that the difference between sides for the surface E_K was significant ($P > 0.05$, Supplementary Table S2). For the photophysiological parameters, both the uncorrected (Supplementary Fig. S3a and b) and biomass (B, normalized by Chl *a* concentrations) initial slope α^B tended to be steeper in 20 m samples compared to the surface samples. For the WEST stations, α^B ranged from 0.080 to 0.013 in surface samples and from 0.012 to 0.017 in 20 m samples. For the EAST stations, α^B ranged from 0.010 to 0.012 in surface samples and from 0.016 to 0.090 in 20 m samples (Table I). The maximum photosynthetic rate P^B_{max} tended to be higher for surface samples. For the WEST stations, the P^B_{max} ranged from 1.25 to 1.83 in surface samples and from 0.68 to 1.32 in 20 m samples. In contrast, the EAST P^B_{max} was generally lower and ranged from 0.68 to 1.26 in surface samples and from 0.58 to 1.00 in 20 m samples (Table I). The P^B_{max} difference between sides was significant (ANOVA Kruskal–Wallis test $P > 0.05$, Supplementary Table S2). The β^B was on average lower on the eastern side (0.002) compared to the western side (0.024). The difference was not significant, but we note that some higher light samples were missing due to on-board ship constraints. There were no significant correlations between the photophysiological indicators and temperature, salinity or nutrients (Spearman's rank correlation coefficient, not shown).

Pigments over time and depths

Phytoplankton pigments indicated taxonomically diverse communities, with characteristic diatom pigments such fucoxanthin (Fuco) and the green algal Chl *b*, tending to dominate. Peridinin, a marker for many photosynthetic dinoflagellates, fluctuated over the sampling period but averaged around 0.08 μmol L^{-1} per mol Chl *a* on each side and both depths. Similarly, dinoxanthin averaged ca. 0.02 μmol L^{-1} per mol Chl *a* (Supplementary Table S3). Neither pigment was correlated with *in situ* PAR, temperature or salinity. The cyanobacteria marker (myxoxanthophyll) was not detected. The full list of identified pigments, corresponding abbreviations and values corrected by Chl *a* (in mol pigments per mol Chl *a*) including degradation pigments from Chl *a* (pheophytin *a* and *b*, pyropheophorbide *a*) are given in Supplementary Table S3.

In general, similar major ancillary pigments were found on both sides of the North Water, but the relative concentrations after normalization varied by station, depth and somewhat by sampling time (Fig. 3, Supplementary Table S3). The eastern side had higher relative abundance of pigments associated with diatoms and other red algal chloroplast lineages, e.g. Fuco and Chl *c*. In contrast, the western side had higher proportions of Chl *b* and Pras typically found in chlorophyte lineages. Micromonal, characteristic of *Micromonas*, concentrations were 3-fold greater in the WEST stations compared to the EAST stations (ca. 0.3 versus 0.1 mol L^{-1} per mol Chl *a*; Supplementary Table S3). Fucoxanthin and co-correlated pigments were relatively lower in the surface compared to the 20 m samples for both WEST and EAST stations. For both sides, the Chl *a* normalized concentrations of taxon-specific pigments varied little within the respective sides for the surface samples over the 24-h sampling. The 20 m depth samples had greater variability over time for both sides of the region (Supplementary Table S4) but reflected the surface with a dominance of the chlorophyte-signature pigment Chl *b* and associated accessory pigments (Supplementary Fig. S5) on the western side (except for T_1) and the red algal lineage pigments such as Fuco and other accessory pigments on the eastern side. An exception on the eastern side was seen in the higher concentrations of Chl *b* at T_3 and T_4 (Fig. 3, Table I, Supplementary Table S3).

One or both of the XC-specific markers for physiological photoprotection using the DES inferred from the DD and the VAZ cycles tended to follow the incoming radiation over the 24 h (Fig. 4), except for the 20 m WEST stations. Correlations (linear regression) were significant for both indicators in the surface of EAST stations, with $R = 0.97$ for DD versus PAR and $R = 0.81$ for VAZ versus PAR, and for the WEST stations, surface DD versus PAR was significant with $R = 0.86$. At 20 m, DD and PAR were significantly correlated for the EAST stations with $R = 0.91$ (Supplementary Fig. S6).

Phytoplankton taxa at 20 m

Since one of our aims was to examine pigments in primarily photosynthetic groups that we could match with marker rRNA data, we excluded dinoflagellates from the taxonomic comparisons because of the high

Downloaded from https://academic.oup.com/plankt/article/43/2/126/6174319 by guest on 19 April 2024

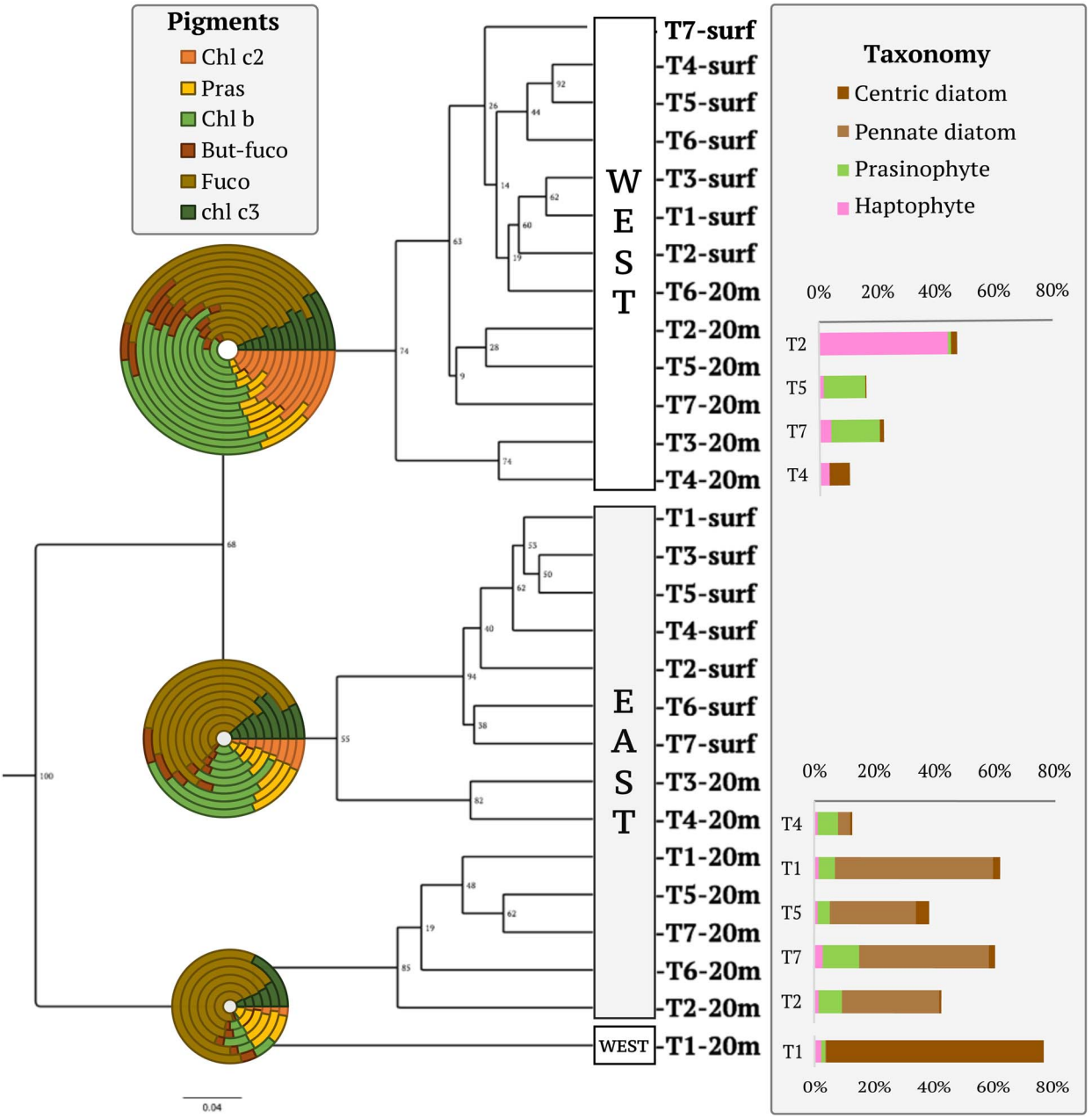

Fig. 3. Samples clustered using Bray–Curtis distance based on pigments that were normalized to Chl *a*. The circular graphs at the nodes show the contribution of taxonomically characteristic pigments for the clusters on the right of the node; circles are arranged following the same order shown in the tree, with the first (top) sample corresponding to the innermost circle and the last sample of the cluster shown as the outermost circle for each of the nodes. The bar graphs show phytoplankton groups as a percentage of total metabarcoding reads from the sample and time of collection; these are positioned closest to the pigment data from the corresponding sample. Taxonomic read data were only available for the 20 m samples at five time points for each side.

proportion on non-photosynthetic taxa or taxa with non-*Peridinium* plastids (Joli *et al*., 2018). The remaining three photosynthetic groups were diatoms, haptophytes and green algae, which accounted for 6–76% of total eukaryote community reads on the western side and 14–54% on the eastern side (Fig. 3). Phytoplankton OTUs with ≥1% relative read abundance in one or more of the samples were identified to the lowest taxonomic level possible (Supplementary Table S5) as in Joli *et al*. (2018). The major photosynthetic taxa were *Pseudo-nitzschia* spp. (Bacillariophyceae), *Chaetoceros gelidus* and *C. neogracilis* (Mediophyceae), *Phaeocystis* and

Downloaded from https://academic.oup.com/plankt/article/43/2/126/6174319 by guest on 19 April 2024

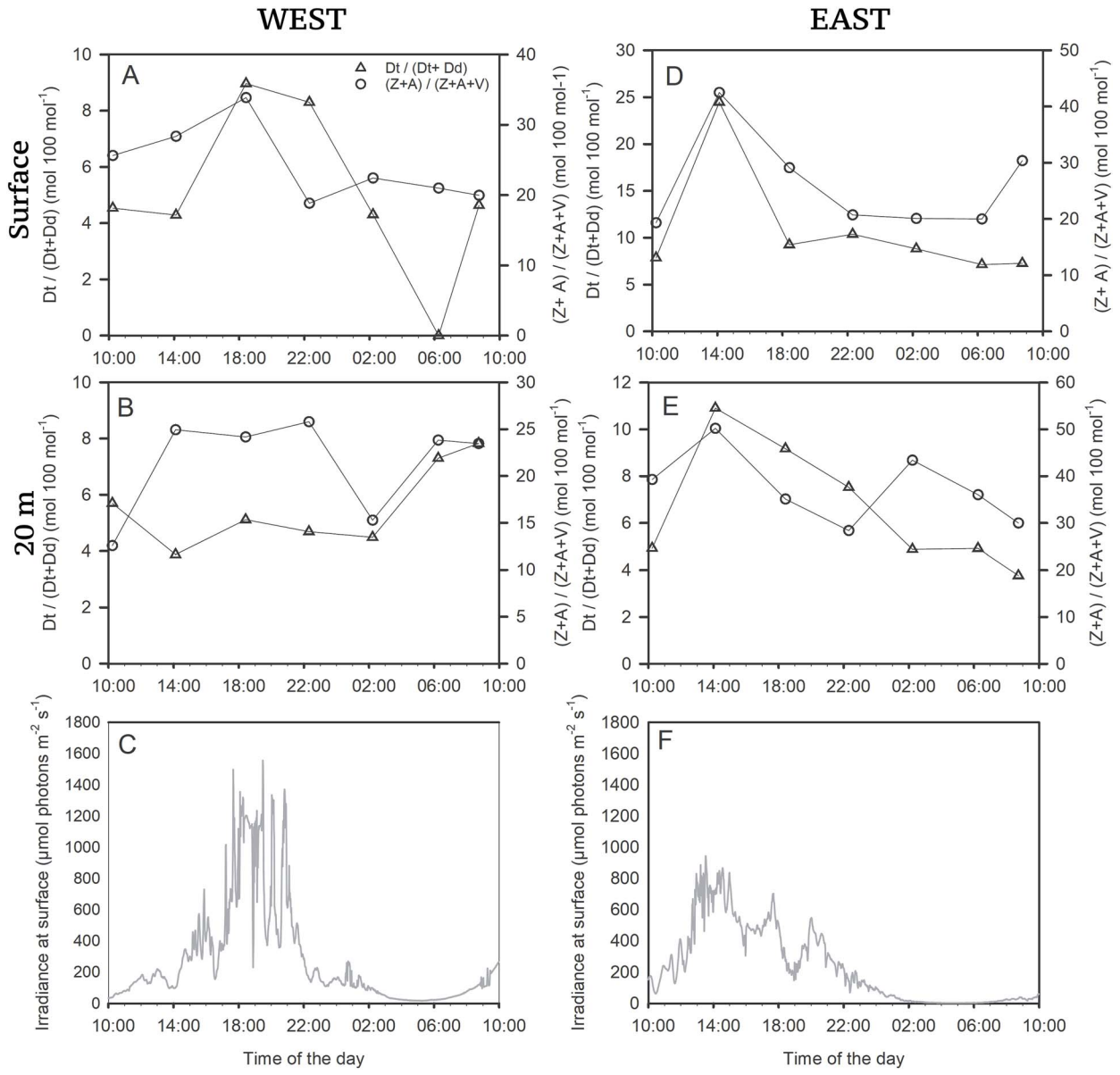

Fig. 4. Time-dependent change in DD as Dt/(Dt + Dd) × 100 (triangles) and in VAZ as (Z + A)/(Z + A + V) (circles) during the day at the surface (upper panels) and at 20 m (middle panels) for WEST stations (A, B, C) and EAST stations (D, E, F). The grey lines (lower panels) are the irradiance values taken from the weather deck on top of the ships bridge. Time is in UTC, local solar time was around UTC–4 h.

Chrysochromulina (Haptophyceae) and Arctic *Pyramimonas* and *Micromonas* (Chlorophyceae). In general, the proportions of different taxa from read abundance varied more on the western side compared to the eastern side (Supplementary Table S6). On the western side, *C. gelidus* was a clear dominant at T_1, while *Phaeocystis* dominated at T_2. *Micromonas polaris* had highest relative abundance at T_5 and T_7. On the eastern side, *Pseudo-nitzschia* spp. had very high relative abundance, with up to 52% of reads, except at T_4. At that time, *Pseudo-nitzschia* proportions fell to <4%, with *M. polaris* and the *Pyramimonas* sp. relatively more common, but the majority of reads were from heterotrophic taxa, especially ciliates (Joli *et al*., 2018).

The pigment signatures and taxa at 20 m depth were examined by canonical correlation analysis (CCA) where complementary data sets existed (T_1, T_2, T_4, T_5 and T_7). In general, the two sides clustered separately along the first axis, which distinguished the diatom especially *Pseudo-nitzschia*-dominated communities of EAST stations from *Micromonas*- and haptophyte-dominated communities of

Downloaded from https://academic.oup.com/plankt/article/43/2/126/6174319 by guest on 19 April 2024

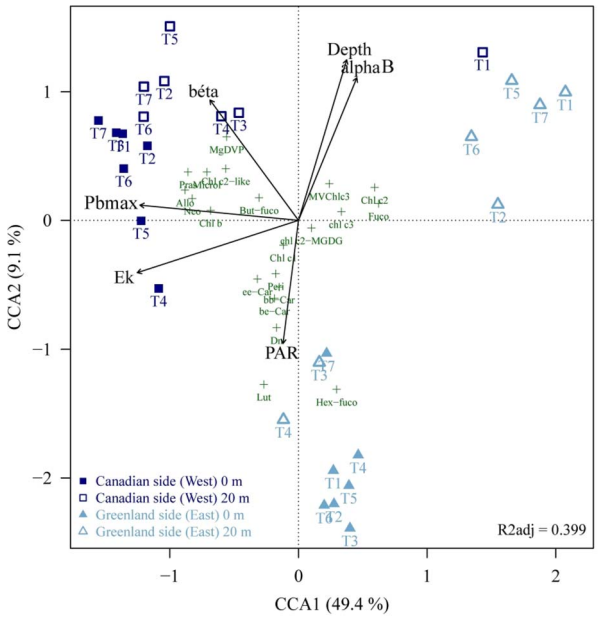

Fig. 5. Canonical correlation analysis (CCA). Arrows represent the photophysiological parameters E_K, α^B (alphaB), β^B (beta) and P^B_{max} (Pbmax) and the abiotic parameters depth and PAR, which were associated with the different samples clustered by pigment content (Chl *a* normalized concentrations of ancillary pigments shown). The CCA was performed using *Vegan* package in R (v.3.4.2) and R studio (v.1.1.419).

WEST stations. The CCA confirmed that the EAST side samples were defined by the presences of Fuco and Chl *c2* with *Pseudo-nitzschia* significantly contributing to the first axis. The second axis highlighted the influence of *C. gelidus* and Chl *c3* from the WEST T_1 sample (Supplementary Fig. S7, Supplementary Table S7). Examining the WEST stations, except for T_1, the vectors followed the pigments found in *Micromonas* (Micro, Chl *b*) but none of the tested taxa statistically contributed.

Pigments and photophysiological indicators

Our main CCA explored the relationship between all the samples from both depths and from T_1 to T_7 with the photophysiological parameters E_K, α^B, P^B_{max} and β^B (Fig. 5) and with the abiotic parameters depth and PAR. The CCA indicated that samples with chlorophyte and haptophyte pigments (e.g. Chl *b* and But-fuco) tended to be associated with a higher E_K and P^B_{max} (Axis − 1). On the other hand, samples with diatom-associated pigments (Fuco, Chl *c2*) were associated with a higher alpha. The second axis was consistent with depth and PAR separating the surface and 20 m samples (Supplementary Table S7).

DISCUSSION

Species-assigned pigments and photosynthetic capacities

Different taxa have characteristic antennae pigments with some used for photoprotection and others tuned to specific underwater light spectra for tailored photon capture associated with depth attenuation. Diatoms often dominate spring blooms under conditions of relatively high light and turbulence (mixing) (Margalef, 1978) associated with nutrient supply (Villamaña *et al.*, 2019). At both depths, there were a higher relative abundance of pigments associated with diatoms in the EAST stations compared to WEST stations, except for the WEST T_1 at 20 m. The use of sequencing showed that there were very different diatom communities on the two sides, suggesting different selection mechanisms. Horizontal advective currents and turbulence may have supplied injections of nitrate and silicate to the *C. gelidus* on the western side (Booth *et al.*, 2002) and nutrient supply from the upwelling north flowing West Greenland Current along with potential micronutrient input favoring *Pseudo-nitzschia* on the eastern side (Joli *et al.*, 2018).

Overall, there was a good match between major taxonomic groups from the sequencing data and characteristic pigments of major phytoplankton groups. The pigments representative of diatoms (Fuco, Chl *c2* and Chl *c3*) were dominant where diatoms were found and pigments associated with *Micromonas* and *Pyramimonas* (Pras and Chl *b*) and haptophytes *Chrysochromulina* and *Phaeocystis* (But-fuco), where these taxa were found (Fig. 3, Supplementary Fig. S7). These associations suggest that similar pigments in the surface waters were associated with the same major groups, and we can assume that generally diatoms were in the surface waters of the EAST stations and small flagellates such as *Micromonas*, *Phaeocystis* and *Chrysochromulina* dominated surface waters of the WEST stations (Fig. 3, Supplementary Fig. S7).

The differences in major groups could also explain the resulting photosynthetic parameters of the community. For the WEST surface, the Chl *a* normalized concentrations for Chl *b* was 2–3 times greater with corresponding higher E_K and P^B_{max} compared to the EAST, despite similar MLDs and average in situ PAR (Table I). Although this could reflect different light and mixing histories, photosynthetic parameters are also reported to be influenced by community composition (Dimier *et al.*, 2009; Bouman *et al.*, 2018), which would be indicated by our results. The role of taxonomy is further supported by photophysiological parameters (E_K, α^B and P^B_{max}) that varied slightly over the 24-h periods within each depth and station but without significant correlations with *in situ* PAR, temperature, salinity or nutrients,

Downloaded from https://academic.oup.com/plankt/article/43/2/126/6174319 by guest on 19 April 2024

consistent with a community change rather than an intrinsic temporal change. Overall, in surface samples, the higher P^B_{max} tracked E_K in keeping with E_K-dependent variation. However, P^B_{max} was not associated with time of day or direct photoacclimation, and differences between sides and depths were associated with community composition. Surface samples from the WEST stations, which were associated with the chlorophyte and haptophyte pigments, had the highest E_K among the four conditions (surface and 20 m for the two sides). This contrasts with previous studies suggesting that the light-saturated photosynthetic coefficient (E_K) tends to be higher where diatoms are dominant compared to flagellates (Huot *et al*., 2013; Fragoso *et al*., 2016). However, in those studies, high P^B_{max}, E_K and diatom abundance may have reflected the higher nutrient concentrations characteristic of the start of the spring bloom dominated by diatoms. In our case, nutrients were low in surface water, and the mixed flagellate community would have an advantage by being better able to use recycled nutrients, e.g. the smaller surface-to-volume ratio for *Micromonas*, which is less than 2 μm diameter, and the likely mixotrophic haptophytes able to gain nutrients from taking up bacteria.

Although E_K did not suggest strong photoacclimation over the day, the DD XC (but not the VAZ) was sensitive to the 24-hour irradiance cycle in surface WEST samples. This would suggest that the haptophytes and less abundant chrysophytes in the surface employed this photoprotective strategy but not *Micromonas*, which was likely the dominant green algae present, as indicated by the concentrations of micromonal (Latasa *et al*., 2004; Supplementary Table S3). The DD cycle was also employed at both surface and 20 m in the EAST stations, supporting the notion that the 20 m and surface communities were more similar to each other in terms of both taxonomy and light history compared to the WEST stations. This would be consistent with exchange between the top of the pycnocline around 20 m (Fig. 2) and the surface waters, leading to mixed layer homogenization. The DD signal and similar E_K values between the surface and 20 m suggest that the *Pseudo-nitzschia* was acclimated to surface conditions in keeping with an active mixed layer. But we cannot rule out that some surface origin cells may also have been deeper due to recent sinking. The VAZ cycle was also employed in surface samples from eastern side (albeit with an R of 0.81, compared to an R of 0.97 for the DD cycle) (Supplementary Fig. S4), which could also reflect taxonomic differences among the chlorophytes, e.g. the presence of more *Pyramimonas*, with an active VAZ cycle (van Leeuwe *et al*. 2005) compared to *Micromonas* on the western side.

Hydrography and photosynthetic parameters

Light fields rapidly change with depth due to selective attenuation of light by water, suspended particles and CDOM (Mobley *et al*., 1994). The surface communities here were photoacclimated with generally higher light-saturation coefficient (E_K) and maximum photosynthetic rate (P^B_{max}) values, compared to 20 m samples (Fig. 1, Table I). On the western side of the North Water, the surface layer is perturbed by the fresher south flowing Arctic water displacing local surface waters along lines of equal density creating interleaved water masses (Lovejoy *et al*., 2002), (Supplementary Fig. S1, Fig. 2). In this context, the phytoplankton are trapped in a given water mass subjected to a light regime that differs from where the community would have originated. The brief occurrence of *Chaetoceros* in the first 20 m sample at this station (WEST T_1) showed a slightly higher α^B compared to other 20 m samples and suggested the capacity to optimize light capture. However, cell numbers from FCM were also minimal in this sample (Supplementary Fig. S2), and *C. gelidus* was not part of a phytoplankton bloom; a mismatch between light and nutrient availability was likely in progress. Although higher fCDOM concentration on the western side might also act to decrease light even near the surface layers (Fig. 2), PAR was similar on both sides of the polynya (Table I), suggesting a minimal effect by fCDOM in the upper 20 m.

Photoacclimation in the PML

As seen in the sub-Antarctic (Doblin *et al*., 2011), photosynthetic parameters measured in the surface were relatively uniform on both sides over the day. Photoacclimation corresponds to several cellular processes that occur over a broad range of time scales, from seconds to days. The parameters of the PE curves (E_K, P^B_{max}) typically respond to the irradiance in time scale of days while the induction of XC can be very fast (seconds to minutes) (Brunet *et al*., 2011). XC is one of the most important photoprotection mechanisms in photosynthetic organisms (Demmig-Adams, 1990; Masojídek *et al*., 2004; Brunet and Lavaud, 2010; Goss and Jakob, 2010) shielding plastids from over-excitation of the photosynthetic pigments and over-reduction of the electron transport chain. The North Water surface XC roughly followed the daily irradiance, and the XC adjustment was consistent with laboratory studies showing that diatoms from the polar region preferentially rely on the XC (and NPQ) to reduce the excitation pressure on Photo System II (Lacour *et al*., 2018). The

Downloaded from https://academic.oup.com/plankt/article/43/2/126/6174319 by guest on 19 April 2024

weaker response of the XC in the 20 m samples likely reflected acclimation to the lower light at this depth and less need for photoprotection. In contrast, the eastern communities with a DD ratio 2.5-fold greater than for the western ones were consistent with a higher need for photoprotection due to the more robust stratification regime with the upper mixed surface layer separated from denser waters below. This intrinsic photoprotection capacity will be essential for long-term survival of Arctic ecotypes, given scenarios with increased stratification and longer ice-free summers, which are inevitable given the current rate of change for the Arctic Ocean (Lee et al. 2016). However, in a scenario of progressive ice loss in the Arctic, one can postulate that prolonged high light conditions will become more and more frequent in addition to nutrient-limiting conditions due to the accumulation of fresh water on the surface. Here, we found higher E_K for small flagellates compared to diatoms in such conditions, which suggests that diatoms will not be able to adapt to high light as well as small flagellates. Our results may partially explain the reasons for the decline of diatoms in at least one Arctic region in recent years (Li et al., 2009).

Model estimates of global and local primary production perform better when *in situ* estimates over regions and depths are available (Campbell *et al*., 2002; Richardson *et al*., 2016) but often are highly reliant on large-scale surface chlorophyll trends and underlying assumptions based on studies mostly from outside of the Arctic (Álvarez *et al*., 2019). Our integrative study, where we investigated short-term variability in polar phytoplankton is unique. We found that despite 24-h light cycle, there is sufficient change in light penetration consistent with the daily change in sun angle that the phytoplankton in the surface adjusted XC photophysiological parameters over the 24 h similar to temperate systems (Bruyant *et al*., 2005). The light history of the cells also had some impact on their photosynthetic capacity, with higher saturation rates of photosynthesis (E_K) for communities under higher light as suggested previously (Brunet *et al*., 2011, Lewis *et al*., 2019). Although not examined here, the weak subsurface chlorophyll maximum (SCM) on the western side was in contrast to an SCM at the top of the nitracline on the eastern side (Joli *et al*., 2018). The two sides represent two alternative scenarios for the Arctic Ocean. The first with a deepening of the nitracline due to freshwater input as seen in the WEST stations (Tremblay *et al*., 2015) and the second, EAST stations, influenced by the biological and physical 'Atlantification' of the Arctic Ocean (Polyakov *et al*., 2018; Oziel *et al*., 2020). This would occur as Atlantic water moves north along the coast of Greenland potentially warming the entire water column, making temperature rather than salinity more likely to be the main factor resulting in stratification. However, in this area, the increasing melt of the Greenland ice sheet will complexify changes in the Arctic seascape. Our study highlights how phytoplankton at the base of the food web could respond to these changes in terms of both taxonomy and photophysiology. This variability in the photophysiological response of marine phytoplankton in Arctic waters should be considered in the estimation of Arctic marine primary production using satellite data in the region.

CONCLUSION

Predicting the photosynthetic efficiency of phytoplankton cells remains one of the major challenges in determining Arctic primary production. Here, we have shown that phytoplankton communities can be replaced by other autotrophic or mixotrophic species under high-flow regimes or adapt to *in situ* conditions where the surface mixed layer is maintained by a strong halocline. Our study provides insight into how physical processes could have an impact on species selection and photoadaptation in Arctic waters.

AUTHOR CONTRIBUTION

N.J. and C.L. designed the study, N.J., T.L. and S.-J.R. carried out the fieldwork and on-board ship data collection. N.J. was responsible for laboratory work and data analysis with input from C.L., N.J.F. and T.L. M.B. contributed facilities for measuring photophysiological parameters. N.J. and C.L. wrote the manuscript; all authors contributed and commented on the various versions of the manuscript.

DATA ARCHIVING

All amplicon results are in the NCBI GenBank Sequence Read Archive under BioProject PRJNA383398. Oceanographic data are available from Amundsen Science: Amundsen Science Data Collection. [2013]. Processed data. Version 1. Archived at www.polardata.ca, Canadian Cryospheric Information Network (CCIN), Waterloo, Canada. doi: 10.5884/12713. Accessed on July 2019.

SUPPLEMENTARY DATA

Supplementary data can be found at *Journal of Plankton Research* online.

ACKNOWLEDGEMENTS

This study is a contribution to ArcticNet, a Network of Centers of Excellence (Canada). We thank P. Guillot for processing CTD

Downloaded from https://academic.oup.com/plankt/article/43/2/126/6174319 by guest on 19 April 2024

data and J. Ferland and J. Larivière for field assistance along with J. Gagnon and G. Deslongchamps, who also provided nutrient data supervised by J.-É. Tremblay. F. Bruyant provided advice on the photophysiological analysis. M.-J. Martineau and W.F. Vincent provided the HPLC data and expertise for data interpretation. Above water daily PAR data were kindly provided by Dr Tim Papakyriakou, University of Manitoba. We also thank R. Logares for bioinformatics support and M. Potvin for processing FCM samples and other laboratory assistance. We acknowledge the contribution by the officers and crew of the Canadian research icebreaker CCGS Amundsen. The data collected by the CCGS Amundsen were made available by the Amundsen Science program, supported by the Canada Foundation for Innovation and NSERC.

FUNDING

N.J. received scholarships from Université Laval and funds from the Canadian Excellence Research Chair (CERC) 'Remote Sensing of Canada's New Arctic Frontier' to M.B. Additional support came from a Natural Sciences and Engineering Research Council of Canada (NSERC) Discovery and Northern Supplement to C.L. and the ArcticNet project Arc3Bio. Additional support was by way of the Fonds de recherche du Québec Nature et Technologies (FRQNT) for Québec-Océan. We acknowledge computing support through Comput Canada.

REFERENCES

Alou-Font, E., Roy, S., Agusti, S. and Gosselin, M. (2016) Cell viability, pigments and photosynthetic performance of Arctic phytoplankton in contrasting ice-covered and open-water conditions during the spring-summer transition. *Mar. Ecol. Prog. Ser.*, **543**, 89–106.

Álvarez, E., Thoms, S., Bracher, A., Liu, Y. and Völker, C. (2019) Modeling photoprotection at global scale: the relative role of non-photosynthetic pigments, physiological state and species composition. *Global Biogeochem. Cycles*, **33**, 904–926.

Anning, T., MacIntyre, H. L., Pratt, S. M., Sammes, P. J., Gibb, S. and Geider, R. J. (2000) Photoacclimation in the marine diatom *Skeletonema costatum*. *Limnol. Oceanogr.*, **45**, 1807–1817.

Apple, J. K., Strom, S. L., Palenik, B. and Brahamsha, B. (2011) Variability in protist grazing and growth on different marine *Synechococcus* isolates. *Appl. Environ. Microbiol.*, **77**, 3074–3084.

Ardyna, M., Gosselin, M., Michel, C., Poulin, M. and Tremblay, J.-É. (2011) Environmental forcing of phytoplankton community structure and function in the Canadian high Arctic: contrasting oligotrophic and eutrophic regions. *Mar. Ecol. Prog. Ser.*, **442**, 37–57.

Arrigo, K. R., Mills, M. M., Kropuenske, L. R., VAN Dijken, G. L., Alderkamp, A. C. and Robinson, D. H. (2010) Photophysiology in two major Southern Ocean phytoplankton taxa: photosynthesis and growth of *Phaeocystis antarctica* and *Fragilariopsis cylindrus* under different irradiance levels. *Int. Comp. Biol.*, **50**, 950–966.

Bâcle, J., Carmack, E. C. and Ingram, R. G. (2002) Water column structure and circulation under the north water during spring transition: April–July 1998. *Deep-Sea Res. II Top. Stud. Oceanogr.*, **49**, 4907–4925.

Belzile, C., Brugel, S., Nozais, C., Gratton, Y. and Demers, S. (2008) Variations of the abundance and nucleic acid content of heterotrophic bacteria in Beaufort shelf waters during winter and spring. *J. Mar. Syst.*, **74**, 946–956.

Blais, M., Ardyna, M., Gosselin, M., Dumont, D., Bélanger, S., Tremblay, J.-É., Gratton, Y., Marchese, C. *et al.* (2017) Contrasting interannual changes in phytoplankton productivity and community structure in the coastal Canadian Arctic Ocean. *Limnol. Oceanogr.*, **62**, 2480–2497.

Booth, B. C., Larouche, P., Bélanger, S., Klein, B., Amiel, D. and Mei, Z. P. (2002) Dynamics of *Chaetoceros socialis* blooms in the north water. *Deep-Sea Res. II Top. Stud. Oceanogr.*, **49**, 5003–5025.

Bouman, H. A., Platt, T., Doblin, M., Figueiras, F. G., Gudmundsson, K., Gudfinnsson, H. G., Huang, B. Q., Hickman, A. *et al.* (2018) Photosynthesis–irradiance parameters of marine phytoplankton: synthesis of a global data set. *Earth Syst. Sci. Data*, **10**, 251–266.

Bouman, H. A., Jackson, T., Sathyendranath, S. and Platt, T. (2020) Vertical structure in chlorophyll profiles: influence on primary production in the Arctic Ocean. *Philos. Trans. Royal Soc A*, **378**, 20190351.

Brunet, C. and Lavaud, J. (2010) Can the xanthophyll cycle help extract the essence of the microalgal functional response to a variable light environment? *J. Plankton Res.*, **32**, 1600–1617.

Brunet, C., Johnsen, G., Lavaud, J. and Roy, S. (2011) Pigments and photoacclimation processes. In Roy, S., Llewellyn, C. A., Egeland, E. S. and Johnsen, G. (eds.), *Phytoplankton Pigments: Characterization, Chemotaxonomy and Applications in Oceanography*, Cambridge University Press, Cambridge, U.K., pp. 445–471.

Bruyant, F., Babin, M., Genty, B., Prasil, O., Behrenfeld, M. J., Claustre, H., Bricaud, A., Garczarek, L. *et al.* (2005) Diel variations in the photosynthetic parameters of *Prochlorococcus* strain PCC 9511: combined effects of light and cell cycle. *Limnol. Oceanogr.*, **50**, 850–863.

Cai, X. and Gao, K. (2015) Levels of daily light doses under changed day-night cycles regulate temporal segregation of photosynthesis and N_2 fixation in the cyanobacterium *Trichodesmium erythraeum* IMS101. *PLoS One*, **10**, e0135401.

Campbell, J., Antoine, D., Armstrong, R., Arrigo, K., Balch, W., Barber, R., Behrenfeld, M. and Bidigare, R. (2002) Comparison of algorithms for estimating ocean primary production from surface chlorophyll, temperature, and irradiance. *Global Biogeochem. Cycles*, **16**, 1035.

Demmig-Adams, B. (1990) Carotenoids and photoprotection in plants: a role for the xanthophyll zeaxanthin. *Biochim. Biophys. Acta (BBA)-Bioenergetics*, **1020**, 1–24.

Dimier, C., Giovanni, S., Ferdinando, T. and Brunet, C. (2009) Comparative ecophysiology of the xanthophyll cycle in six marine phytoplanktonic species. *Protist*, **160**, 397–411.

Doblin, M. A., Petrou, K. L., Shelly, K., Westwood, K., Van den Enden, R., Wright, S., Griffiths, B., and Ralph, P. J. (2011). Diel variation of chlorophyll-*a* fluorescence, phytoplankton pigments and productivity in the Sub-Antarctic and Polar Front Zones south of Tasmania, Australia. *Deep Sea Res., Part II*, **58**, 2189–2199.

Dron, A., Rabouille, S., Claquin, P., Le Roy, B., Talec, A. and Sciandra, A. (2012) Light dark (12:12) cycle of carbon and nitrogen metabolism in *Crocosphaera watsonii* WH8501: relation to the cell cycle. *Environ. Microbiol.*, **14**, 967–981.

Dupont, C. L., McCrow, J. P., Valas, R., Moustafa, A., Walworth, N., Goodenough, U., Roth, R., Hogle, S. L. *et al.* (2015) Genomes and gene expression across light and productivity gradients in eastern subtropical Pacific microbial communities. *ISME J.*, **9**, 1076–1092.

Edgar, R. C. (2013) UPARSE: highly accurate OTU sequences from microbial amplicon reads. *Nature Meth.*, **10**, 996–998.

Edwards, K. F., Thomas, M. K., Klausmeier, C. A. and Litchman, E. (2015) Light and growth in marine phytoplankton: allometric, taxonomic, and environmental variation. *Limnol. Oceangr.*, **60**, 540–552.

Downloaded from https://academic.oup.com/plankt/article/43/2/126/6174319 by guest on 19 April 2024

Fragoso, G. M., Poulton, A. J., Yashayaev, I. M., Head, E. J. H., Stinchcombe, M. C. and Purdie, D. A. (2016) Biogeographical patterns and environmental controls of phytoplankton communities from contrasting hydrographical zones of the Labrador Sea. *Prog. Oceanogr.*, **141**, 212–226.

Goss, R. and Jakob, T. (2010) Regulation and function of xanthophyll cycle-dependent photoprotection in algae. *Photosynth. Res.*, **106**, 103–122.

Goss, R. and Lepetit, B. (2015) Biodiversity of NPQ. *J. Plant Physiol.*, **172**, 13–32.

Grasshoff, K., Kremling, K. and Ehrhardt, M. (2009) *Methods of Seawater Analysis, Third Edition*, John Wiley and Sons, Weinheim, Germany.

Harding, L. W., Prézelin, B. B., Sweeney, B. M. and Cox, J. L. (1981) Diel oscillations in the photosynthesis-irradiance relationship of a planktonic marine diatom. *J. Phycol.*, **17**, 389–394.

Heide-Jørgensen, M. P., Burt, L. M., Hansen, R. G., Nielsen, N. H., Rasmussen, M., Fossette, S. and Stern, H. (2013) The significance of the north water polynya to arctic top predators. *Ambio*, **42**, 596–610.

Herzig, R. and Dubinsky, Z. (1993) Effect of photoacclimation on the energy partitioning between cyclic and non-cyclic photophosphorylation. *New Phytol.*, **123**, 665–672.

Huang, T.-C., Tu, J., Chow, T.-J. and Chen, T.-H. (1990) Circadian rhythm of the prokaryote *Synechococcus* sp. RF-1. *Plant Physiol.*, **92**, 531–533.

Huot, Y., Babin, M. and Bruyant, F. (2013) Photosynthetic parameters in the Beaufort Sea in relation to the phytoplankton community structure. *Biogeosciences*, **10**, 3445–3454.

Huot, Y., Babin, M., Bruyant, F., Grob, C., Twardowski, M. S. and Claustre, H. (2007) Relationship between photosynthetic parameters and different proxies of phytoplankton biomass in the subtropical ocean. *Biogeosciences*, **4**, 853–868.

Joli, N., Gosselin, M., Ardyna, M., Babin, M., Onda, D. F., Tremblay, J.–. É. and Lovejoy, C. (2018) Need for focus on microbial species following ice melt and changing freshwater regimes in a Janus Arctic gateway. *Sci. Rep.*, **8**, 9405.

Kalenitchenko, D., Joli, N., Potvin, M., Tremblay, J. E. and Lovejoy, C. (2019) Biodiversity and species change in the Arctic Ocean: a view through the lens of Nares Strait. *Front. Mar. Sci.*, **6**, UNSP 479.

Karnovsky, N. J. and Hunt, G. L. (2002) Estimation of carbon flux to dovekies (*Alle alle*) in the north water. *Deep-Sea Res: Part II*, **49**, 5117–5130.

Kavanaugh, M. T., Oliver, M. J., Chavez, F. P., Letelier, R. M., Muller-Karger, F. E. and Doney, S. C. (2016) Seascapes as a new vernacular for pelagic ocean monitoring, management and conservation. *ICES J. Mar. Sci.*, **73**, 1839–1850.

Lacour, T., Larivière, J. and Babin, M. (2017) Growth, Chl *a* content, photosynthesis, and elemental composition in polar and temperate microalgae. *Limnol. Oceanogr.*, **62**, 43–58.

Lacour, T., Larivière, J., Ferland, J., Bruant, F., Lavaud, J. and Babin, M. (2018) The role of sustained photoprotective non-photochemical quenching in low temperature and high light acclimation in the bloom-forming Arctic diatom *Thalassiosira gravida*. *Front. Mar. Sci.*, **5**, 354.

Latasa, M., Scharek, R., Gall, F. L. and Guillou, L. (2004) Pigment suites and taxonomic groups in Prasinophyceae. *J. Phycol.*, **40**, 1149–1155.

Lee, Y. J., Matrai, P. A., Friedrichs, M. A. M., Saba, V. S., Aumont, O., Babin, M., Buitenhuis, E. T. and Chevallier, M. (2016) Net primary productivity estimates and environmental variables in the Arctic Ocean: an assessment of coupled physical-biogeochemical models. *J. Geophys. Res. Ocean.*, **121**, 8635–8669.

Lewis, K. M., Arntsen, A. E., Coupel, P., Joy-Warren, H., Lowry, K. E., Matsuoka, A., Mills, M. M., VAN Dijken, G. L. *et al.* (2019) Photoacclimation of Arctic Ocean phytoplankton to shifting light and nutrient limitation. *Limnol. Oceanogr.*, **64**, 285–301.

Li, W. K. W., McLaughlin, F., Lovejoy, C. and Carmack, E. (2009) Smallest algae thrive as the Arctic Ocean freshens. *Science*, **326**, 539–539.

Logares, R. (2017) UPARSE workflow for MiSeq amplicons. v1.5. Available at: https://github.com/ramalok/amplicon_processing.

Lovejoy, C., Carmack, E. C., Legendre, L. and Price, N. M. (2002) Water column interleaving: a new physical mechanism determining protist communities and bacterial states. *Limnol. Oceanogr.*, **47**, 1819–1831.

Marchese, C., Albouy, C., Tremblay, J.-É., Dumont, D., D'Ortenzio, F., Vissault, S. and Bélanger, S. (2017) Changes in phytoplankton bloom phenology over the north water (NOW) polynya: a response to changing environmental conditions. *Polar Biol.*, **40**, 1721–1737.

Martin, J., Tremblay, J. É., Gagnon, J., Tremblay, G., Lapoussière, A., Jose, C., Poulin, M., Gosselin, M. *et al.* (2010) Prevalence, structure and properties of subsurface chlorophyll maxima in Canadian Arctic waters. *Mar. Ecol. Prog. Ser.*, **412**, 69–84.

Margalef, R. (1978) Life-forms of phytoplankton as survival alternatives in an unstable environment. *Oceanol. Acta*, **1**, 493–509.

Masojidek, J., Kopecká, J., Koblížek, M. and Torzillo, G. (2004) The xanthophyll cycle in green algae (Chlorophyta): its role in the photosynthetic apparatus. *Plant Biol.*, **6**, 342–349.

Mobley, C. D. (1994) *Light and Water: Radiative Transfer in Natural Waters*, Academic Press, San Diego.

Monier, A., Comte, J., Babin, M., Forest, A., Matsuoka, A. and Lovejoy, C. (2015) Oceanographic structure drives the assembly processes of microbial eukaryotic communities. *ISME J.*, **9**, 990–1002.

Ottesen, E. A., Young, C. R., Eppley, J. M., Ryan, J. P., Chavez, F. P., Scholin, C. A. and DeLong, E. F. (2013) Pattern and synchrony of gene expression among sympatric marine microbial populations. *Proc. Natl. Acad. Sci. U. S. A.*, **110**, E488–E497.

Oziel, L., Baudena, A., Ardyna, M., Massicotte, P., Randelhoff, A., Sallée, J. B., Ingvaldsen, R. B., Devred, E. *et al.* (2020) Faster Atlantic currents drive poleward expansion of temperate phytoplankton in the Arctic Ocean. *Nature Com.*, **11**, 1705.

Polyakov, I. V., Pnyushkov, A. V. and Carmack, E. (2018) Stability of the arctic halocline; a new indicator of arctic climate change. *Environ. Res. Lett.*, **13**, 125008.

Raven, J. A. and Geider, R. J. (2003) Adaptation, acclimation and regulation in algal photosynthesis. In Larkum, A. W. D., Douglas, S. E. and Raven, J. A. (eds.), *Photosynthesis in Algae. Advances in Photosynthesis and Respiration*, Vol. **14**, Springer, Dordrecht, pp. 385–412.

Richardson, K., Bendtsen, J., Kragh, T. and Mousing, E. A. (2016) Constraining the distribution of photosynthetic parameters in the Global Ocean. *Front. Mar. Sci.*, **3**, UNSP269.

Roy, S., Llewellyn, C. A., Egeland, E. S. and Johnsen, G. (eds.) (2011) *Phytoplankton Pigments: Characterization, Chemotaxonomy and Applications in Oceanography*, Cambridge University Press, Cambridge.

Russo, A. D., DE Souza, M. S., Mendes, C. R. B., Tavano, V. M. and Garcia, C. A. E. (2018) Spatial variability of photophysiology and

Downloaded from https://academic.oup.com/plankt/article/43/2/126/6174319 by guest on 19 April 2024

primary production rates of the phytoplankton communities across the western Antarctic peninsula in late summer 2013. *Deep-Sea Res. II Top. Stud. Oceanogr.*, **149**, 99–110.

Sakshaug, E., Bricaud, A., Dandonneau, Y., Falkowski, P. G., Kiefer, D. A., Legendre, L., Morel, A., Parslow, J. *et al.* (1997) Parameters of photosynthesis: definitions, theory and interpretation of results. *J. Plankton Res.*, **19**, 1637–1670.

Salazar, G., Paoli, L., Alberti, A., Huerta-Cepas, J., Ruscheweyh, H. J., Cuenca, M., Field, C. M., Coelho, L. P. *et al.* (2019) Gene expression changes and community turnover differentially shape the Global Ocean metatranscriptome. *Cell*, **179**, 1068–1083.

Tremblay, J. É., Anderson, L. G., Matrai, P., Coupel, P., Bélanger, S., Michel, C. and Reigstad, M. (2015) Global and regional drivers of nutrient supply, primary production and CO_2 drawdown in the changing Arctic Ocean. *Prog. Oceanogr.*, **139**, 171–196.

van de Poll, W. H., Maat, D. S., Fischer, P., Rozema, P. D., Daly, O. B., Koppell, S., Visser, R. J. W. and Buma, A. G. J. (2016) Phytoplankton chlorophyll-*a* and taxonomic composition in Kongsfjorden, Spitsbergen. *Front. Mar. Sci.*, **3**, UNSP200.

Van Leeuwe, M., Van Sikkelerus, B., Gieskes, W. and Stefels, J. (2005) Taxon-specific differences in photoacclimation to fluctuating irradiance in an Antarctic diatom and a green flagellate. *Mar. Ecol. Prog. Ser.*, **288**, 9–19.

Villamaña, M., Marañón, E., Cermeño, P., Estrada, M., Fernández-Castro, B., Figueiras, F. G., Latasa, M., Otero-Ferrer, J. L. *et al.* (2019) The role of mixing in controlling resource availability and phytoplankton community composition. *Prog. Oceanogr.*, **178**, 102181.

Zapata, M., Rodríguez, F. and Garrido, J. L. (2000) Separation of chlorophylls and carotenoids from marine phytoplankton: a new HPLC method using a reversed phase C8 column and pyridine-containing mobile phases. *Mar. Ecol. Prog. Ser.*, **195**, 29–45.

Downloaded from https://academic.oup.com/plankt/article/43/2/126/6174319 by guest on 19 April 2024